Functional Nonlinear Mixed Effects Models for Longitudinal Image Data

Xinchao Luo[1,2], Lixing Zhu[3], Linglong Kong[4], and Hongtu Zhu[1(✉)]

[1] Department of Biostatistics and Biomedical Research Imaging Center, University of North Carolina at Chapel Hill, Chapel Hill, USA
htzhu@email.unc.edu
[2] School of Finance and Statistics, East China Normal University, Shanghai, China
[3] Department of Mathematics, Hong Kong Baptist University, Hong Kong, China
[4] Department of Mathematical and Statistical Sciences, University of Alberta, Edmonton, Canada

Abstract. Motivated by studying large-scale longitudinal image data, we propose a novel functional nonlinear mixed effects modeling (FNMEM) framework to model the nonlinear spatial-temporal growth patterns of brain structure and function and their association with covariates of interest (e.g., time or diagnostic status). Our FNMEM explicitly quantifies a random nonlinear association map of individual trajectories. We develop an efficient estimation method to estimate the nonlinear growth function and the covariance operator of the spatial-temporal process. We propose a global test and a simultaneous confidence band for some specific growth patterns. We conduct Monte Carlo simulation to examine the finite-sample performance of the proposed procedures. We apply FNMEM to investigate the spatial-temporal dynamics of white-matter fiber skeletons in a national database for autism research. Our FNMEM may provide a valuable tool for charting the developmental trajectories of various neuropsychiatric and neurodegenerative disorders.

Keywords: Functional nonlinear mixed effects model · Functional response · Global test statistic · Simultaneous confidence band · Spatial-temporal pattern

1 Introduction

Improving understanding of brain structure and function (e.g., brain circuits) can be translated to the study of various neuropsychiatric and neurodegenerative disorders [2,3,5,9,10,14]. In effect, it is common to collect big data with great complexity and diversity in order to understand how changes in the brain

Lixing Zhu was supported by a grant from the University Grants Council of Hong Kong, China.

Hongtu Zhu was partially supported by NIH grants MH086633, RR025747, and MH092335 and NSF grants SES-1357666 and DMS-1407655.

S. Ourselin et al. (Eds.): IPMI 2015, LNCS 9123, pp. 794–805, 2015.
DOI: 10.1007/978-3-319-19992-4_63

can lead to these brain-related disorders and to understand their trajectories across the lifespan and across diverse populations. By learning more about such trajectories, one hopes to improve existing approaches and devise new ones for the prevention, treatment, and cure of such disorders. To accomplish these objectives, development of novel statistical methods and their software platforms are critically important to deal with difficulties and challenges inherent in imaging data and associated data obtained from large-scale biomedical studies.

The aim of this paper is to develop a FNMEM framework to delineate dynamic changes of longitudinal image data and their association with a set of covariates of interest and to characterize their large spatial-temporal variations. The FMPM framework is motivated by the emerging demand to analyze massive image data collected in large-scale longitudinal biomedical studies, such as the Alzeimer's disease neuroimaging initiative [12]. In those studies, longitudinal functional data from different subjects, denoted by $\{y_{ij}(s) = y_i(t_{ij}, s) : i = 1, \cdots, n\}$, are usually observed and/or normalized in a large number of locations of a common space, denoted by $\mathcal{S}$, across multiple time points $\{t_{ij} : j = 1, \cdots, T_i\}_{i \geq 1}$. Also, $\mathcal{S}$ is often a compact subset of Euclidean space.

Methodology to handle longitudinal image data is still in its infancy, and further theoretical and practical development is much needed. Most existing methods focus on the analysis of univariate (or multivariate) variables measured longitudinally [4]. Many parametric mixed effects models including both fixed and random effects are the predominant approach for characterizing both the temporal correlations and random individual variations. Although there is a great interest in the analysis of functional data with various levels of hierarchical structures [7,11,18], only a handful of them [6,17,21] focused on the development of linear mixed models for longitudinal image data. Recently, there was some attempt on the development of hierarchical geodesic models on diffeomorphism for longitudinal shape analysis [15].

Specifically, FNMEM contains two major components including a random nonlinear association map for characterizing dynamic association between image data and covariates, and a spatial-temporal process for capturing large subject variation across both spatial and temporal domains. Because of its greater flexibility, FNMEM is generally more interpretable and parsimonious, and the predictions obtained from FNMEM extend more reliably outside the observed range of the data. We explicitly incorporate the spatial-temporal smoothness into our estimation procedure in order to accurately estimate the nonlinear association map and the spatial-temporal covariance operator. We also propose a global test statistic for testing the association map and construct its asymptotic simultaneous confidence band.

2 Method

2.1 Functional Nonlinear Mixed Effects Model

A functional nonlinear mixed effects model consists of two major components. The first one is a pointwise nonlinear mixed effects model given by

$$y_{ij}(s) = f(\phi_i(s), \mathbf{x}_{ij}) + \varepsilon_{ij}(s) \quad \text{for} \quad i = 1, \ldots, n, \tag{1}$$

where $f(\cdots)$ is a real-valued, differentiable nonlinear association map, $\phi_i(s)$ is a $p \times 1$ vector of subject-specific functions, $\mathbf{x}_{ij}$ is p-dimensional covariate of interest, and $\varepsilon_i(s)$ is the corresponding random error process. It is assumed that f has continuous second-order derivative with respect to $\phi_i(s)$. For image data, it is typical that after normalization, $y_{ij}(s)$ are measured at the same location for all subjects and exhibit both the within curve and between-curve dependence structure. Thus, without loss of generality, it is assumed that $y_{ij}(s)$ are observed on the M same grid points $\mathcal{S}_0 = [0,1] = \{s_m, 0 = s_1 \leq s_2 \cdots \leq s_M = 1\}$ for all subjects and time points.

The second one is a spatial-temporal process for modeling large variations across subject-specific functions $\phi_i(s)$. Specifically, $\phi_i(s)$ is modeled as

$$\phi_i(s) = \beta(s) + b_i(s), \tag{2}$$

where $\beta(\cdot) = (\beta_1(\cdot), \cdots, \beta_p(\cdot))^T$ is a $p \times 1$ vector of fixed effect functions and $b_i(s) = (b_{i1}(s), \cdots, b_{ip}(s))^T$ is a $p \times 1$ vector of random effect functions. In addition, $\{b_i(s)\}$ and $\{\varepsilon_i(s)\}$ are independent and identical copies of SP(0, $\Sigma_b(s,t)$) and SP(0, $\sigma_\varepsilon^2(s)1(s=t)$) respectively, where SP($\mu(s)$, $\Sigma(s,t)$) is a stochastic process (e.g., Gaussian process) with mean function $\mu(s)$ and covariance function $\Sigma(s,t)$.

2.2 An Example

Recently, nonlinear mixed effects models based on the Gompertz function have been used to characterize longitudinal white matter development during early childhood [3,9,14] The Gompertz function can be written as

$$y = f(\phi, t) = \textbf{asymptote}\ \exp(-\textbf{delay}\ \exp(-\textbf{speed}\ t)) = \phi_1 \exp\{-\phi_2 \phi_3^t\},$$

where ϕ_1 is asymptote, ϕ_2 is delay, and ϕ_3 is exp(−speed). Specifically, in [14], a nonlinear mixed effects model based on the Gompertz function is given by

$$y_{ij} = \phi_{1i} \exp\{-\phi_{2i} \phi_{3i}^{t_{ij}}\} + \varepsilon_{ij} \quad \text{and} \quad \phi_i = (\phi_{1i}, \phi_{2i}, \phi_{3i})^T = \beta + b_i, \tag{3}$$

where $\beta = (\beta_1, \beta_2, \beta_3)^T$ are fixed effects and b_i are random effects. For image data, an extension of model (3) is to consider a FNMEM as

$$y_{ij}(s) = \phi_{1i}(s) \exp\{-\phi_{2i}(s) \phi_{3i}(s)^{t_{ij}}\} + \varepsilon_{ij}(s) \quad \text{and} \quad \phi_i(s) = \beta(s) + b_i(s). \tag{4}$$

We will use model (4) to characterize the spatial-temporal dynamics of white-matter fiber tracts.

2.3 Estimation Procedure

The next interesting question is how to estimate the fixed effect and random effect functions of FNMEM. It should be noted that the estimation procedures used in [6,17,21] are not directly applicable here due to the nonlinear association map in (1).

Estimating the Fixed Effect Functions. At each grid point $s_m \in \mathcal{S}_0$, we treat model (1) as a traditional nonlinear mixed effects model as

$$y_{ij}(s_m) = f(\beta(s_m) + b_i(s_m), \mathbf{x}_{ij}) + \varepsilon_{ij}(s_m), \tag{5}$$

where $b_i(s_m) \sim N(0,\ \Sigma_b(s_m, s_m))$ and $\varepsilon_{ij}(s_m) \sim N(0,\ \sigma^2(s_m))$. Then, we calculate the maximum likelihood estimator of $\beta(s_m)$, denoted by $\hat{\beta}(s_m)$, across all s_m. Define $K_h(t-s) = K((t-s)/h)/h$ as the kernel function, where K is the Epanechnikov kernel, and $\tilde{K}_h(s_m - s) = K_h(s_m - s)/\{\sum_{m=1}^{M} K_h(s_m - s)\}$. We calculate a kernel estimator of $\beta(s)$ as:

$$\tilde{\beta}(s) = \sum_{m=1}^{M} \tilde{K}_{h_1}(s_m - s)\hat{\beta}(s_m) \quad \text{for all} \quad s \in \mathcal{S}. \tag{6}$$

The bandwidth $\hat{h}_1$ is selected using a leave-one-out cross-validation method.

Estimating the Covariance Operators. Under certain smoothness conditions on $b_i(s)$, we use local linear regression technique to estimate all $b_i(s)$. Specifically, by using Taylor expansion for $b_i(s_m)$ at $b_i(s)$, we have

$$b_i(s_m) \approx b_i(s) + \dot{b}_i(s)(s_m - s) = B_i(s)Z(s_m - s),$$

where $B_i(s) = (b_i(s), \dot{b}_i(s))$ is a $p \times 2$ matrix and $Z(s_m - s) = (1, (s_m - s))^T$ is a p dimensional vector, in which $\dot{b}_i(s) = (\dot{b}_{i1}(s), \cdots, \dot{b}_{ip}(s))^T$ and $\dot{b}_{il}(s) = \partial b_{il}(s)/\partial s$ for $l = 1, \cdots, p$. For each i and s, we estimate $B_i(s)$ by minimizing the weighted nonlinear least squares [19]:

$$S_M(B_i(s)) \stackrel{\text{def}}{=} \sum_{j=1}^{n_i} \sum_{m=1}^{M} \left\{ y_{ij}(s_m) - f(\hat{\beta}(s_m) + B_i(s)Z(s_m - s), \mathbf{x}_{ij}) \right\}^2 K_{h_2}(s_m - s).$$

The optimal bandwidth $\hat{h}_2$ is selected using a leave-one-out cross-validation method, and an iteration algorithm is proposed to get the estimators. Finally, let $N = \sum_{i=1}^{n} n_i$, we estimate $\Sigma_b(s,t)$ by using

$$\hat{\Sigma}_b(s,t) = N^{-1} \sum_{i=1}^{n} n_i \tilde{b}_i(s)\tilde{b}_i(t)^T.$$

Functional Principal Component Analysis. With the empirical covariance $\hat{\Sigma}_b(s,t)$, we follow [13] and calculate the spectral decomposition as

$$\hat{\Sigma}_b(s,t) = \sum_{k=1}^{\infty} \hat{\lambda}_k \hat{\psi}_k(s)\hat{\psi}_k(t)^T,$$

where $\hat{\lambda}_k$ are estimated eigenvalues and $\hat{\psi}_k(s)$ are their corresponding estimated eigenfunctions. Moreover, the k-th functional principal component scores can be computes by $\hat{\xi}_{ik} = \sum_{m=1}^{M} \tilde{b}_i(s_m)\psi_k(s_m)(s_m - s_{m-1})$ for $i = 1, \cdots, n$.

2.4 Inference Procedure

The next interesting question is how to make statistical inference on the fixed effect functions of FNMEM.

Hypothesis Test. We focus on the linear hypothesis of $\beta(s)$ as follows

$$H_0: \ R\beta(s) = \mathbf{b}_0(s) \text{ for all } s \qquad \text{vs.} \qquad H_1: \ R\beta(s) \neq \mathbf{b}_0(s),$$

where R is a $r \times p$ matrix with rank r, and b_0 is a given $r \times 1$ vector of functions. A global test statistic S_n is given by

$$S_n = \int_0^1 \mathbf{d}(s)^T [R\hat{\Sigma}(s,s)R^T]^{-1}\mathbf{d}(s)ds,$$

where $\mathbf{d}(s) = R[\tilde{\beta}(s) - \text{bias}(\tilde{\beta}(s))] - \mathbf{b}_0(s)$, $\hat{\Sigma}(s,s) = \widehat{\text{Var}(\tilde{\beta}(s))}$. We just drop $\text{bias}(\tilde{\beta}(s))$ when calculate the score functions for computational efficiency since $R\tilde{\beta}(s) \approx \mathbf{b}_0(s)$ and $\text{bias}(\tilde{\beta}(s)) = o_p(h_1^2)$, so that $R\text{bias}(\tilde{\beta}(s)) \approx \mathbf{0}$. Since the asymptotic distribution of S_n is very complicated, we can hardly approximate the percentiles of S_n under H_0 directly. Instead, we propose a score bootstrap method [8] to obtain the p value.

Simultaneous Confidence Bands. Give a confidence level α, we construct simultaneous confidence bands for each $\beta_l(s), l = 1, \cdots, p$ as follows:

$$P(\hat{\beta}_l^{L,\alpha}(s) < \beta_l(s) < \hat{\beta}_l^{U,\alpha}(s) \text{ for all } s \in \mathcal{S}) = 1 - \alpha,$$

where $\hat{\beta}_l^{L,\alpha}(s)$ and $\hat{\beta}_l^{U,\alpha}(s)$ are the lower and upper limits of simultaneous confidence band, respectively. We develop a resampling method to approximate the bounds as in [19].

3 Numerical Studies

In this section, we use Monte Carlo simulations and a real example to evaluate the finite sample performance of FNMEM.

3.1 Simulations

We generated multiple data sets from a FNMEM given by

$$y_{ij}(s) = \exp\{x_{ij1}\phi_{1i}(s) + x_{ij2}\phi_{2i}(s)\} + \varepsilon_i(s) \quad \text{and} \quad \phi_{li}(s) = \beta_l(s) + b_{li}(s)$$

for $l = 1, 2$, $j = 1, \cdots, n_i$ and $i = 1, \cdots, n$. We use two sets of simulations to investigate the estimation and inference procedures.

Simulation 1. The first one is to evaluate the power of the global test statistic S_n. Let s_m be equidistant time points in $[0,1]$, where $s_1 = 0$ and $s_M = 1$. Moreover, $\varepsilon_{ij}(s) \sim N(0, 0.1)$ and $(x_{ij1}, x_{ij2})^T \sim N((0,0)^T, \Sigma)$ with $\Sigma = (\sigma_{jk})_{p\times p}$, where $\sigma_{jk} = 0.3^{|k-j|}$ for $1 \leqslant k, j \leqslant p$. Furthermore, we set $b_i(s)$ as

$$b_i(s) = \sin(2\pi s) \cdot N((0,0)^T, 0.1 \times \Sigma) + \cos(2\pi s) \cdot N((0,0)^T, 0.2 \times \Sigma).$$

The functional fixed effects functions $\beta(s)$ are given by

$$\beta_1(s) = cs^2 \quad \text{and} \quad \beta_2(s) = (1-s)^2.$$

To examine the hypothesis test $H_0 : \beta_1(s) = 0$ for all s against $H_1 : \beta_1(s) \neq 0$ for at least one s, we set c at different values in order to study the Type I error rates and power. Specifically, we fixed $c = 0$ to assess the Type I error, and then set $c = 0.05, 0.1, 0.15, 0.2$ to examine the power of S_n. We set $M = 25$ and $n_i = 5$. To evaluate at different sample sizes, we set $n = 50$ and 100 for each c. We calculated the rejection rate under the significance levels $\alpha = 0.05$ and 0.01 by using the score bootstrap method with $G = 500$. 200 replications are used for each simulation setting.

Figure 1 shows the power curves at two different significance levels. It can be seen that Type I error rates based on score bootstrap are well maintained under the pre-fixed significance levels when $n = 100$. The power of rejecting the null hypothesis increases with the sample size as expected. To show that FNMEM outperforms voxel-wise NMEM, we estimated $\hat{\Sigma}(s_m, s_m)$ using the asymptotic covariance matrix without smoothing, and then calculated the global testing statistic and its p-values with the score bootstrap method as in FNMEM. Figure 1 shows that voxel-wise NMEM is much less powerful than FNMEM.

Simulation 2. The second one is to explore the finite-sample performance of simultaneous confidence band. We used the same data generation procedure as Simulation 1. We fix $c = 1$ and then set $n = 50$, $n_i = 5$, $M = 25$, 50 and 75. Based on 200 replications, we calculated simultaneous confidence bands for each component of $\beta(s)$ by using the wild bootstrap method with $G = 500$. Table 1 summarizes the empirical coverage probabilities for $\alpha = 0.05$ and 0.01. Again as expected, with the number of grid points M increasing, the coverage probabilities are improved. When $M = 75$, the results are reasonable since the coverage probabilities are quite closed to the prespecified confidence levels $1 - \alpha$. The Monte Carlo errors are of size $\sqrt{0.95 \times 0.05/200} \approx 0.015$ for $\alpha = 0.05$. Figure 2 presents typical 95 % and 99 % simultaneous confidence bands for $M = 75$.

3.2 Real Data Analysis

We analyzed a data set taken from a national database for autism research (NDAR) (http://ndar.nih.gov/), an NIH-funded research data repository, that aims to accelerate progress in autism spectrum disorders (ASD) research through data sharing, data harmonization, and the reporting of research results. 416 high quality MRI scans are available for 253 children (126 males and 127 females) with 45 grid points, demographic information is shown in Table 2.

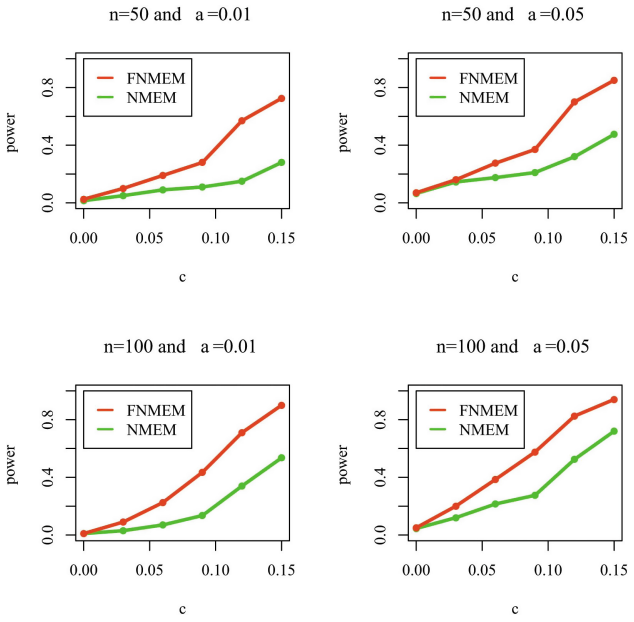

Fig. 1. Plots of power curves. Rejection rates of S_n based on score bootstrap method are calculated at six different values of c using FNMEM and NMEM, with sample size 50 and 100 at significance levels 5 % and 1 %.

Table 1. Empirical coverage probabilities of $1 - \alpha$ simultaneous confidence bands for all components of β based on 200 simulated data sets.

M	β_1	β_2	β_1	β_2
	$\alpha = 0.05$		$\alpha = 0.01$	
25	0.935	0.925	0.975	0.975
50	0.935	0.930	0.980	0.980
75	0.950	0.945	0.985	0.990

The data were processed by two key steps including a weighted least squares estimation method [1]; [20] to construct the diffusion tensors and a FSL TBSS pipeline [16] to register DTIs from multiple subjects to create a mean image and a mean skeleton. Specifically, maps of fractional anisotropy (FA) were computed for all subjects from the DTI after eddy current correction and automatic brain extraction using FMRIB software library. FA maps were then fed into the TBSS tool, which is also part of the FSL. In the TBSS analysis, the FA data of all the subjects were aligned into a common space by non-linear registration and the mean FA image were created and thinned to obtain a mean FA skeleton, which represents the centers of all WM tracts common to the group. Subsequently, each subjects aligned FA data were projected onto this skeleton.

We focus on the midsagittal corpus callosum skeleton and associated FA curves. The corpus callosum (CC) is the largest fiber tract in the human brain and is a topographically organized structure. It is responsible for much of the

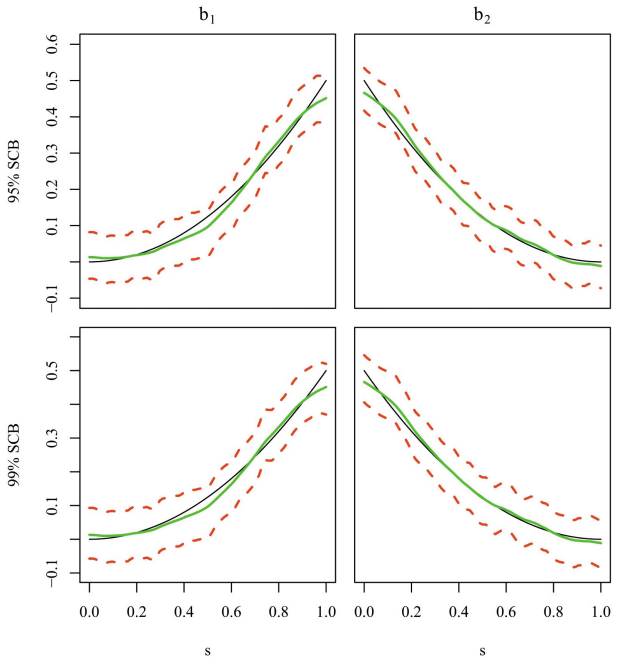

Fig. 2. Typical 95 % (the first row) and 99 % (the second row) simultaneous confidence bands for $M = 75$. The black solid, green solid, and red dash curves are, respectively, the true curves, the estimated curves and their corresponding 95 % and 99 % simultaneous confidence bands (Color figure online).

Table 2. Demographic information for participants.

Visit	Number of subjects	Age(years)	Range(years)
1	58	10.53(5.96)	[0, 18]
2	148	12.25(4.62)	[0, 21]
3	160	12.29(5.14)	[1, 22]
4	19	1.84(1.42)	[1, 6]
5	7	1.57(0.79)	[1, 3]
6	10	2.70(0.67)	[2, 4]
7	6	3.17(0.75)	[2, 4]
8	5	3.40(1.14)	[2, 5]
9	3	3.67(1.15)	[3, 5]
Gender	Male/Female		126/127

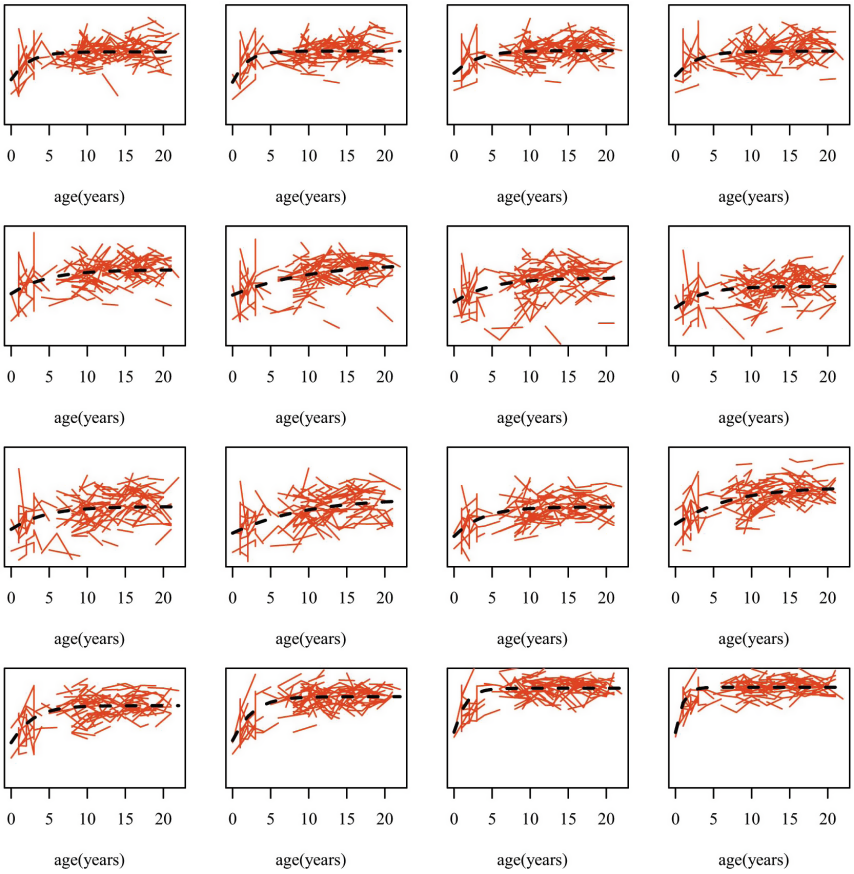

Fig. 3. Tract (red solid lines) varying as a function of age for grid points from 25 to 40, the black dash curves are estimated curves (Color figure online).

communication between the two hemispheres and connects homologous areas in the two cerebral hemispheres.

Figure 3 shows the variations of tract as age increases for grid points from 25 to 40, as well as the estimated curves at these grid points. It is observed that there are random subject-to-subject variations at each grid point along this tract as well as random subject-to-subject variations in the age effect at the selected location.

We fitted model (4) to the real data. We estimated the functional fixed effects functions $\beta(s)$ and constructed their 95 % and 99 % simultaneous confidence bands by using wild bootstrap method with $G = 500$ replications. We also constructed the global test statistic S_n to test the significance of delay and speed. The p-value of S_n is approximated by the score bootstrap method with $G = 500$ replications. Figure 5 shows the first 10 eigenvalues and 4 eigenfunctions

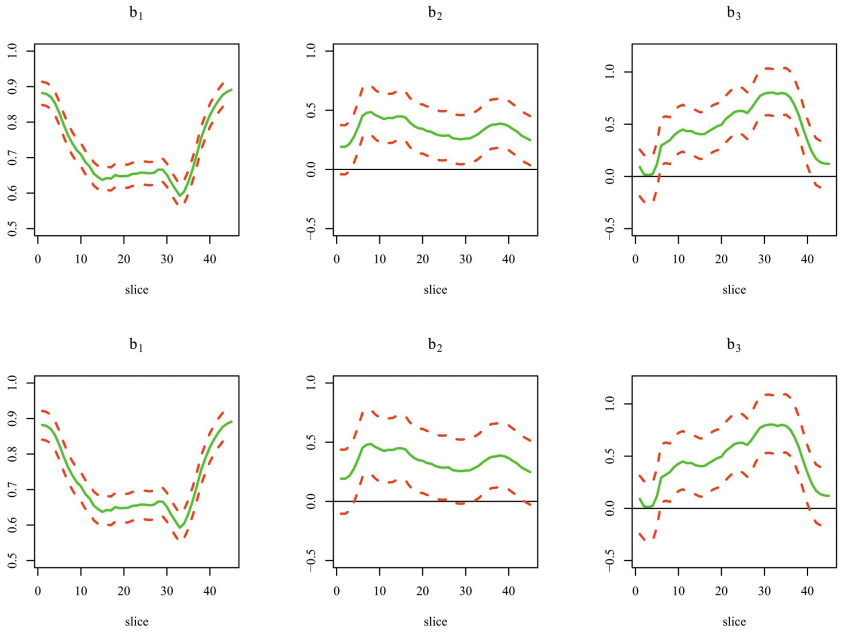

Fig. 4. The $100(1-\alpha)\%$ simultaneous confidence bands of parameters for $\alpha = 0.05$ (the first row) and $\alpha = 0.01$ (the second row). The green solid and red dash curves are, respectively, the estimated curves and their corresponding 95 % and 99 % simultaneous confidence bands (Color figure online).

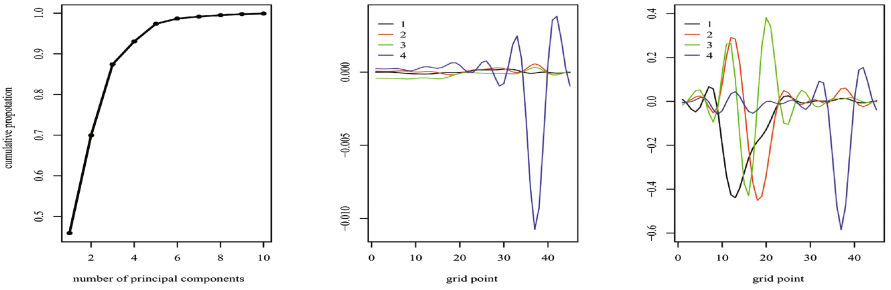

Fig. 5. The $100(1-\alpha)\%$ cumulative proportion of the first 10 eigenvalues (left). The first 4 eigenfunctions corresponding to $b_{i1}(s)$ (middle) and $b_{i2}(s)$ (right).

of $\hat{\Sigma}_b(s,t)$. We can observe that the first four eigenvalues contribute more than 90 % (93.04 %) of the total while the rest quickly vanish to zero.

Figure 4 presents the uncertainty in the estimated coefficient functions, the horizontal line crossing $(0,0)$ is contained. It can be seen that the horizontal lines are under the 95 % simultaneous confidence band of delay coefficients and exp(−speed) coefficients at most of the grid points. In addition, exp(−speed) coefficients are significantly less than 1. These may indicate that the **measures**

will increase with age, but the growth will slow down quickly and then become flat. To test the age effect, we calculated the global test statistic $S_n = 763.73$ and obtained its associated p-value ($p < 0.001$), indicating a significant age effect. Our analysis of simultaneous confidence band also agrees with the hypothesis test results.

References

1. Basser, P.J., Mattiello, J., LeBihan, D.: Estimation of the effective self-diffusion tensor from the nmr spin echo. J. Magn. Resonan. Ser. B **103**(3), 247–254 (1994)
2. Bernal-Rusiel, J., Greve, D., Reuter, M., Fischl, B., Sabuncu, M.R.: Statistical analysis of longitudinal neuroimage data with linear mixed effects models. NeuroImage **66**, 249–260 (2013)
3. Dean, D.C., O'Muircheartaigh, J., Dirks, H., Waskiewicz, N., Walker, L., Doernberg, E., Piryatinsky, I., Deoni, S.C.L.: Characterizing longitudinal white matter development during early childhood. Brain Struct. Funct. (2014, in press)
4. Diggle, P., Heagerty, P., Liang, K.Y., Zeger, S.: Analysis of Longitudinal Data, 2nd edn. Oxford University Press, New York (2002)
5. Gilmore, J.H., Shi, F., Woolson, S., Knickmeyer, R.C., Short, S.J., Lin, W.L., Zhu, H.T., Hamer, R.M., Styner, M., Shen, D.G.: Longitudinal development of cortical and subcortical gray matter from birth to 2 years. Cereb. Cortex **22**, 2478–2485 (2011)
6. Greven, S., Crainiceanu, S., Caffo, B.S., Reich, D.: Longitudinal functional principal component analysis. Electron. J. Stat. **4**, 1022–1054 (2010)
7. Guo, W.: Functional mixed effects models. Biometrics **58**, 121–128 (2002)
8. Kline, P., Santos, A.: A score based approach to wild bootstrap inference. J. Econom. Methods **1**, 23–41 (2012)
9. Kulikova, S., Hertz-Pannier, L., Dehaene-Lambertz, G., Buzmakov, A., Poupon, C., Dubois, J.: Multi-parametric evaluation of the white matter maturation. Brain Struct. Funct. (2014, in press)
10. Lebel, C., Beaulieu, C.: Longitudinal development of human brain wiring continues from childhood into adulthood. J. Neurosci. **31**, 10937–10947 (2011)
11. Morris, J.S., Carroll, R.J.: Wavelet-based functional mixed models. J. R. Stat. Soc. Ser. B Stat. Methodol. **68**, 179–199 (2006)
12. Mueller, S.G., Weiner, M.W., Thal, L.J., Petersen, R.C., Jack, C.R., Jagust, W., Trojanowski, J.Q., Toga, A.W., Beckett, L.: Ways toward an early diagnosis in Alzheimer's disease: the Alzheimer's disease neuroimaging initiative (adni). Alzheimer's Dement. **1**(1), 55–66 (2005)
13. Rice, J.A., Silverman, B.W.: Estimating the mean and covariance structure nonparametrically when the data are curves. J. R. Stat. Soc. Ser. B (Methodol.) **53**, 233–243 (1991)
14. Sadeghi, N., Prastawa, M., Fletcher, P.T., Wolff, J., Gilmore, J.H., Gerig, G.: Regional characterization of longitudinal DT-MRI to study white matter maturation of the early developing brain. NeuroImage **68**, 236–247 (2013)
15. Singh, N., Hinkle, J., Joshi, S., Fletcher, P.T.: A hierarchical geodesic model for diffeomorphic longitudinal shape analysis. In: Gee, J.C., Joshi, S., Pohl, K.M., Wells, W.M., Zöllei, L. (eds.) IPMI 2013. LNCS, vol. 7917, pp. 560–571. Springer, Heidelberg (2013)

16. Smith, S.M., Jenkinson, M., Johansen-Berg, H., Rueckert, D., Nichols, T.E., Mackay, C.E., Watkins, K.E., Ciccarelli, O., Cader, M.Z., Matthews, P.M., et al.: Tract-based spatial statistics: voxelwise analysis of multi-subject diffusion data. Neuroimage **31**(4), 1487–1505 (2006)
17. Yuan, Y., Gilmore, J.H., Geng, X., Styner, M., Chen, K., Wang, J.L., Zhu, H.: Fmem: Functional mixed effects modeling for the analysis of longitudinal white matter tract data. NeuroImage **84**, 753–764 (2014)
18. Zhu, H., Brown, P., Morris, J.: Robust, adaptive functional regression in functional mixed model framework. J. Am. Stat. Assoc. **106**, 1167–1179 (2011)
19. Zhu, H., Li, R., Kong, L.: Multivariate varying coefficient model for functional responses. Ann. Stat. **40**, 2634–2666 (2012)
20. Zhu, H., Zhang, H., Ibrahim, J.G., Peterson, B.S.: Statistical analysis of diffusion tensors in diffusion-weighted magnetic resonance imaging data. J. Am. Stat. Assoc. **102**(480), 1085–1102 (2007)
21. Zipunnikov, V., Greven, S., Shou, H., Caffo, B., Reich, D.S., Crainiceanu, C.: Longitudinal high-dimensional principal components analysis with application to diffusion tensor imaging of multiple sclerosis. Ann. Appl. Stat. (2014, in press)